Letter

Direct link between disorder and magnetoresistance in topological semimetals

Jocienne N. Nelson,[1,*] Ian A. Leahy,[1,*] Anthony D. Rice,[1] Chase Brooks,[2] Glenn Teeter,[1] Mark van Schilfgaarde,[1] Stephan Lany,[1] Brian Fluegel,[1] Minhyea Lee,[2] and Kirstin Alberi[1,†]

[1]*National Renewable Energy Laboratory, Golden, Colorado 80401, USA*

[2]*Department of Physics, University of Colorado, Boulder, Colorado 80309, USA*

(Received 21 June 2022; revised 14 February 2023; accepted 8 June 2023; published 29 June 2023)

The extent to which disorder influences the properties of topological semimetals is relevant to the understanding of topological states and their use in practical applications. Using molecular beam epitaxy, we achieve systematic control of point defect concentrations in the prototypical Dirac semimetal Cd_3As_2 to gain insight into the role of disorder on electron transport behavior. Using the guiding center diffusion model for linear magnetoresistance, we extract point defect densities as a function of deposition conditions. We find that reducing cadmium defect concentrations by an order of magnitude results in an 2× increase in the magnetoresistance from 450% to 900%. This finding yields important information in the quest to identify the origin of linear magnetoresistance in a wider range of materials.

DOI: 10.1103/PhysRevB.107.L220206

Three-dimensional (3D) topological semimetals (TSMs) exhibit linear and gapless bulk band dispersions and topologically protected surface states arising from band inversion [1]. Topological protection against carrier backscattering is thought to support high electron mobilities up to 10^7 cm^2/(V s) in the Dirac semimetal Cd_3As_2 and 10^5–10^6 cm^2/(V s) in the Weyl semimetal family (Ta,Nb)(As,P) [2,3]. TSMs typically feature Fermi levels near the band touching nodes (∼100 meV) coupled with large Fermi velocities, which only occur in systems with nonparabolic bands. Together, these aspects lead to extremely large, nonsaturating linear magnetoresistance (LMR). Several studies argue that disorder is the basis for nonsaturating LMR [4,5] but do not provide a clear picture of the exact mechanisms that influence it or how to tune it. To address this gap, we systematically vary the point defect populations in the prototypical Dirac semimetal Cd_3As_2 to directly obtain information about how disorder influences LMR in TSMs.

The role of disorder in transport behavior is important to understand, as thin-film TSMs are starting to be incorporated into devices. Crystals naturally contain point and extended defects, which are theoretically predicted to introduce potential variations and limit the carrier mean free path [6–9]. However, the quantitative extent to which a specific instance of disorder influences LMR has not been experimentally tested. For example, arsenic vacancies were speculated to influence LMR in Cd_3As_2 based on measurements in a single sample [10], but without a systematic variation, these defects could not be verified as the origin of the LMR, and the magnitude of their effect on LMR could not be derived.

Advances in theoretical models describing the origin of LMR may help to improve our understanding of the disorder-electron transport relationships if we can combine them with a controlled variation of specific instances of disorder. Recently, the guiding center diffusion model (GCDM) has been proposed [11], where the trajectories of charge carriers are altered by a potential landscape induced by small-scale levels of disorder. The GCDM explains the ubiquitous LMR in TSMs without invoking strong inhomogeneity, as required by the resistor model network [4,5], or without the need for quantum limit transport enabling quantum linear MR [12]. Another advantage is its ability to provide quantitative information about disorder based on simple magnetotransport measurements. This model has principally only been applied to single bulk crystals with limited control of disorder, restricting the insights that can be derived. Pairing it with the powerful ability to tune defect populations through thin-film synthesis promises to provide more definitive information about which defects play the biggest role in influencing LMR. Experimental verification of the GCDM in a system with controllable disorder is also necessary for understanding its broader applicability in describing LMR in TSMs.

In this Letter, we link LMR to disorder introduced by charged point defects. Through the use of molecular beam epitaxy (MBE) with separate Cd and As sources, we modify the chemical potential during growth and methodically tune the native defect populations to a degree not available in bulk synthesis. We then extract the strength and average spacing of

*These authors contributed equally to this work.

†Author to whom all correspondence should be addressed: Kirstin.Alberi@nrel.gov

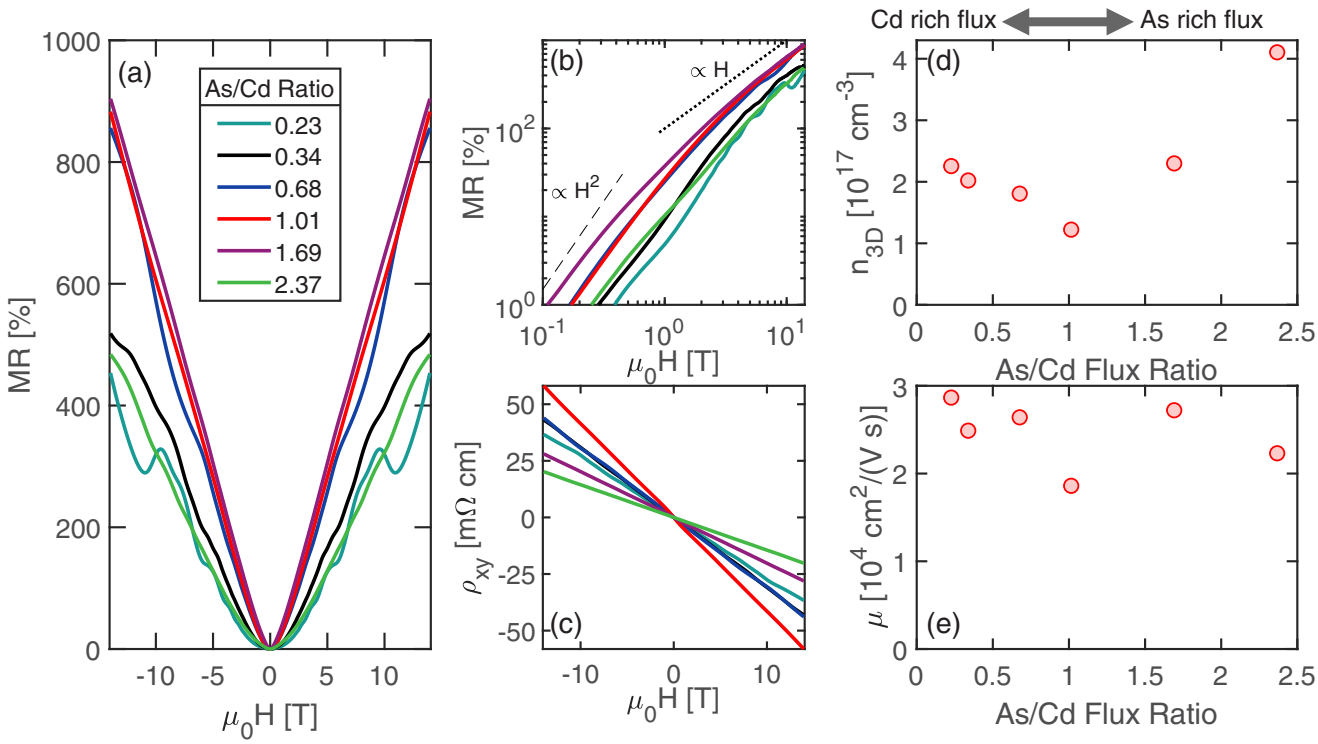

FIG. 1. Electrical transport measurements performed at 2 K. (a) Magnetoresistance % as a function of applied magnetic field $H \parallel \hat{z}$, current $I \parallel \hat{x}$ for Cd_3As_2 samples grown with different As/Cd flux ratios but otherwise under identical conditions. (b) Log-log plot illustrating that the MR for all samples crosses over from quadratic to linear field dependence at an onset field between 1 and 10 T that depends on the As/Cd flux ratio. (c) Hall resistivity as a function of magnetic field for the same samples. (d) Electron concentration n_{3D} and (e) mobility μ as a function of As/Cd flux ratio

this disorder with the GCDM. Combining our findings with density functional theory (DFT), we conclude that charged cadmium defects mainly impact the electrical transport of Cd_3As_2. While these defects introduce modest disorder potentials ∼10–20 meV, lowering their concentration by an order of magnitude leads to a marked increase in the LMR. This work experimentally verifies the GCDM as an accurate predictor of LMR values, positioning it as a tool to evaluate how to tune LMR in other materials.

Cd_3As_2(112) thin films were synthesized at 115 °C on GaAs(111) substrates using light-assisted MBE. All samples have similar thicknesses (490–575 nm). The ratio of the As/Cd fluxes was varied from 0.23 to 2.37. This variation does not influence the stoichiometry at the atomic % level, as verified by x-ray photoemission spectroscopy [Supplemental Material (SM) Fig. S1 [13]] but instead influences the concentration of native point defects at typical electronic doping levels (<0.04%), as typical in semiconductors. Hall bars were fabricated with standard photolithography, wet chemical etching, and electroplated Au contacts. Magnetotransport measurements were performed in a Physical Property Measurement System from Quantum Design. We present a DFT analysis of the intrinsic point defects for the 80-atom ground state structure with spin-orbit coupling to understand how point defects impact the density of states near the Dirac point. Total energies and electronic structures were calculated using the pseudopotential momentum-space formalism, the projector augmented-wave (PAW) method as implemented in the VASP code [14], and the strongly constrained and appropriately normed (SCAN) exchange-correlation functional [15]. SCAN is a meta generalized gradient approximation (meta-GGA) functional in which the local exchange-correlation potential of standard DFT is replaced by a differential operator [16], and it generally improves the description of lattice parameters and electronic properties such as band gaps in semiconductors and insulators [17]. More information on the synthesis, magnetotransport measurements, and calculations are available in the SM [13] (see also Refs. [18–26] therein) and Ref. [27].

Figure 1 presents results demonstrating that the As/Cd flux ratio used during growth significantly impacts the MR properties. All measurements were performed at 2 K. Figure 1(a) shows the MR% defined as $\mathrm{MR\%} = 100\% \times \frac{[\rho_{xx}(\mu_0 H) - \rho_{xx}(\mu_0 H = 0)]}{\rho_{xx}(\mu_0 H = 0)}$, where ρ_{xx} is the longitudinal resistivity, the magnetic field $H \parallel \hat{z}$, and current $I \parallel \hat{x}$. The MR at $\mu_0 H =$ 14 T ranges from 450% in the sample grown under the lowest As/Cd flux ratio (As/Cd = 0.23, teal) to 905% in the sample grown with the nearly highest As/Cd flux ratio (As/Cd = 1.69, purple). This latter value is large compared to 300%–500% values measured in other Cd_3As_2 thin films [28,29], and the total MR% variation across samples is approximately 2×. Furthermore, all samples display a turnover from quadratic to LMR with an onset field between 1 and 10 T that is dependent on As/Cd flux ratio [Fig. 1(b)]. Figure 1(c) shows the Hall resistivity (ρ_{xy}) as a function of applied field. The ρ_{xy} of all samples has a negative slope, suggesting that the transport is dominated by a single electronlike carrier. This is consistent with behavior in bulk crystals and is expected when the Fermi level is pinned above the Dirac node [2,30]. The presence of

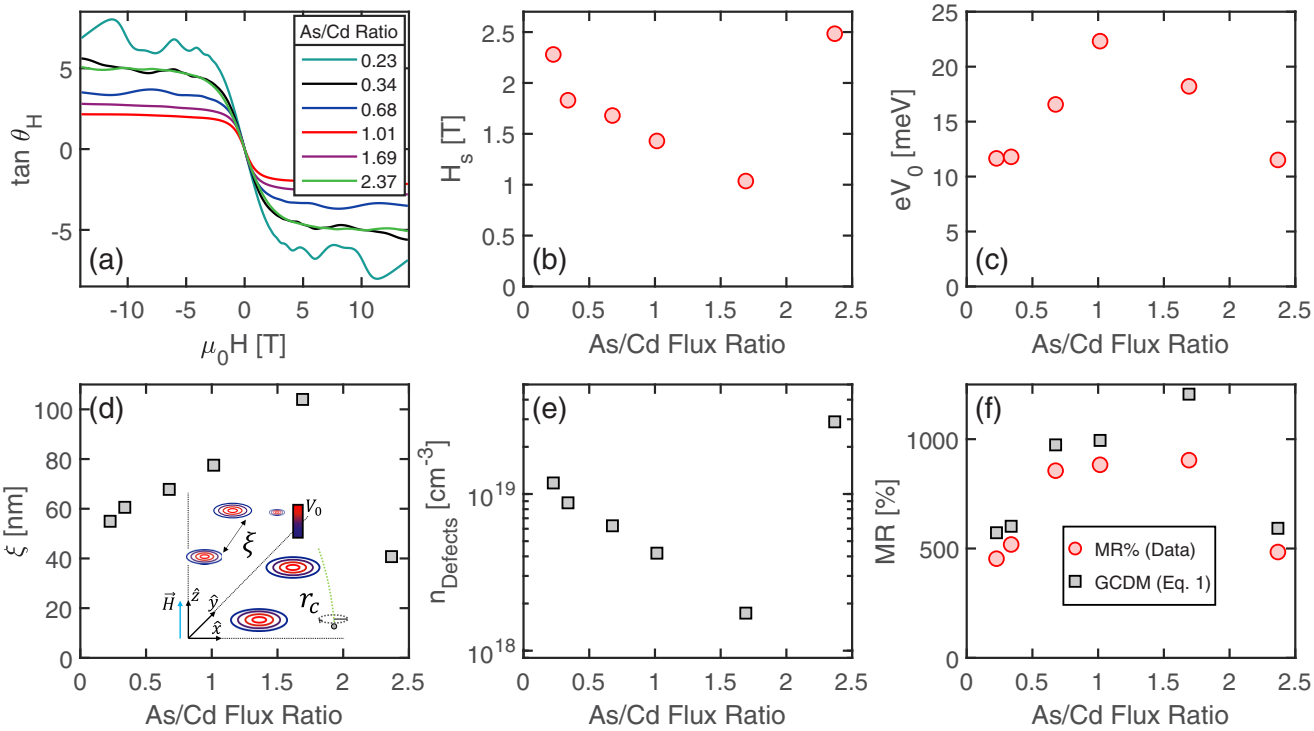

FIG. 2. (a) $\tan\theta_H = \rho_{xy}(H)/\rho_{xx}(H)$ as a function of magnetic field for samples grown under different As/Cd ratios. (b) The field saturation of $\tan\theta_H$ which occurs at field H_S when MR% or equivalently ρ_{xx} becomes linear. (c) The disorder potential eV_0 as a function of As/Cd flux ratio. (d) The disorder length scale ξ determined by the cyclotron radius at the saturation field H_S. The inset shows a simplified schematic of the guiding center diffusion model (GCDM), adapted from Ref. [11], which we use to describe the 3D charge carrier motion. The concentric circles represent samplings of the disorder potential. (e) The density of point defects suggested by the disorder length scale ξ (black squares). We calculate the density of point defects as $n_{\text{Defects}} = (8\alpha^3\xi^3)^{-1}$, where $\alpha \approx 0.04$ is the effective fine-structure constant for Cd_3As_2 [9]. (f) MR% as a function of the As/Cd ratio compared with the predicted MR% from the GCDM [11]. All measurements were performed at 2 K.

Shubnikov–de Haas (SdH) oscillations demonstrates that all samples are of high quality.

Figures 1(d) and 1(e) show carrier concentration n_{3D} and the mobility μ extracted from low-field (± 0.1 T) Hall measurements as a function of As/Cd flux ratio. The transport behavior evolves as a function of As/Cd flux ratio used during growth. The carrier density initially decreases with increasing As/Cd ratio, reaches a minimum value at 1.2×10^{17} cm^{-3} at As/Cd = 1, then increases for more As-rich growth. The mobility for all our samples is large [$>18\,000$ cm^2/(V s)] and does not systematically vary with the flux ratio.

In Fig. 2, we analyze the magnetotransport to quantify the role of disorder, which we will show is key to explaining the changes in the MR% and the carrier concentration trends shown in Fig. 1. Figure 2(a) shows the field dependence of the tangent of the Hall angle, $\tan\theta_H = \frac{\rho_{xy}(H)}{\rho_{xx}(H)}$, measured at 2 K. With increasing field magnitude, we find that $|\tan\theta_H|$ rapidly saturates at a large value ($|\tan\theta_H| > 2$) for all samples. Similar behavior of $\tan\theta_H$ has previously been used to evaluate nonsaturating LMR in TaP and NbP single crystals [31]. In these materials the field saturation of $\tan\theta_H$ was found to be explained by the GCDM [11].

The GCDM does not require multiband compensation or significant disorder to explain the nonsaturating LMR and is the most appropriate framework for Cd_3As_2. A schematic of the GCDM principles is shown in the inset of Fig. 2(d). The 3D trajectories of charge carriers are altered by a smoothly varying potential energy landscape originating from disorder with typical strength V_0 and correlation length ξ. Smoothly varying disorder potentials are generated via the effective screening of charged defects resulting from large dielectric constants in TSMs [9]. LMR in the GCDM arises from the scattering and subsequently altered diffusion of low momentum charge carriers around the disorder potentials. These carriers that scatter and diffuse around the potentials dominate the electrical transport when the cyclotron radius r_c is reduced below the disorder correlation length, yielding LMR. Such disorder potentials have been shown to emerge from charge puddles induced to screen charged defects in Cd_3As_2 and the TSM Na_3Bi [32,33]. These disorder potentials vary on length scales of tens of nanometers, which can satisfy the requisite GCDM ingredient for smoothly varying potentials, $r_c < \xi$, at reasonable fields in many TSMs. In the case of Cd_3As_2, high Fermi velocities ($\sim 10^6$ m/s) [2] and small magnitudes of the Fermi level above the Dirac point (0.1–0.2 eV) suggests that r_c can reach 10–100 nm at modest magnetic fields ($\sim$10 T), permitting us to probe disorder on this length scale. This combination of large Fermi velocity and low Fermi level is common to many other topological materials with nonparabolic bands, highlighting the large scope of applicability of our findings. Analysis of the $\tan\theta_H$ field dependence allows us to quantitatively determine when the MR becomes linear: Because ρ_{xy} is linear over the whole field range studied, $\tan\theta_H$ is field independent once ρ_{xx} becomes linear. We

extract the saturation field H_S by fitting $\tan\theta_H$ to the empirical equation $\tan\theta_H = A\tanh(H/H_S)$, where A is a constant. The extracted H_S, shown in Fig. 2(b), decreases with increasing As/Cd flux ratio except in the most As-rich condition.

From the GCDM framework, we extract the disorder strength eV_0 [Fig. 2(c)], which is predicted to follow the relationship $\tan\theta_H = \frac{2}{\sqrt{27\pi}}\left(\frac{E_F}{eV_0}\right)^{3/2}$ in the regime where $\tan\theta_H$ is field independent (i.e., $H > H_S$) [11]. Here, the Fermi level E_F, extracted from the dominant SdH oscillation frequency [SM Fig. S2(c) [13]], is defined relative to the Dirac point. The disorder strength is maximized for As/Cd = 1 and decreases with As- or Cd-rich growth. The values of eV_0 determined in our Cd_3As_2 epilayers are consistent with scanning tunneling spectroscopy measurements of bulk Cd_3As_2 [32], providing additional evidence that the disorder potentials in topological semimetals are low compared to the thermal energy of electrons that extend up to even modest temperatures. The disorder correlation length can be extracted from the r_c at H_S where the MR% becomes linear: $\xi \approx \frac{m_e^* v_F}{e\mu_0 H_S}$. We assume the Fermi velocity is constant as a function of As/Cd flux ratio and use the value of $v_F = 9.3\times10^5$ m/s from Ref. [2] along with $m_e^* = E_F/v_F^2$ to calculate the disorder correlation length. In Fig. 2(d) we show that ξ estimated from $\tan\theta_H$ increases as a function of the As/Cd flux ratio. Both ξ and V_0 have a similar order of magnitude as found in bulk NbP and TaP [31]. While ξ is a measure of the average distance between maxima in the disorder potential, these maxima are the result of the additive screened potentials of several charged defects. To calculate the charged defect concentration, we utilize the relation $n_{\text{Defects}} = (8\alpha^3\xi^3)^{-1}$ [9] where $\alpha \approx 0.04$ is the effective fine-structure constant for Cd_3As_2 [Fig. 2(e)].

Within the GCDM, MR% is predicted to be related to disorder (via $\tan\theta_H$) by [11]

$$\text{MR\%} \approx \frac{\mu}{10^4}\,\mu_0 H\,\frac{\tan\theta_H}{1+\tan^2\theta_H}, \tag{1}$$

where MR% increases with increasing mobility and increasing V_0 for our Fermi energies (95–115 meV). Figure 2(f) demonstrates that Eq. (1) agrees with our data, verifying the GCDM model. This provides an experimental basis for understanding disorder-driven LMR in a wide variety of TSMs.

Evaluation of the quantitative ξ and V_0 parameters extracted from MR data allows us to conclude that the main source of disorder influencing MR behavior in Cd_3As_2 is native point defects. The disorder length scales imply that scattering centers are located every ~40–100 nm on average, corresponding to point defect densities $\sim10^{18}$–10^{19} cm^{-3}, which could reasonably be expected in our epilayers. On the other hand, threading dislocations would be spaced several hundred nanometers or microns apart for the known densities of mid 10^8 cm^{-2} in our epilayers [27]. We also do not expect the As/Cd flux ratio to influence extended defects in the same way as point defects.

To understand the role of point defect populations in electron transport in Cd_3As_2, we examine their behavior with DFT. The 80-atom primitive cell of the Cd_3As_2 crystal structure (space group $I4_1/acd$) is made up of building blocks of antifluorite Cd_4As_2 with an ordered arrangement of missing Cd atoms (empty sites) [34], as illustrated in Fig. 3(a). Thus, we expect Cd interstitials (Cd_i) and vacancies (V_{Cd})

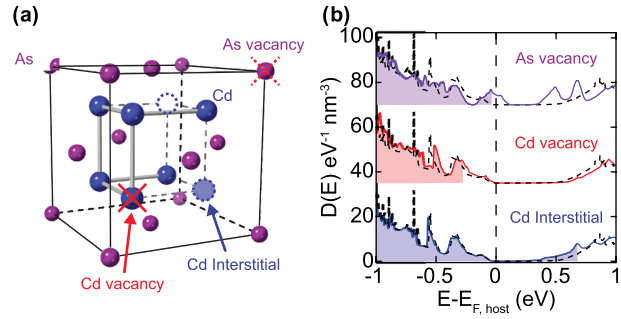

FIG. 3. (a) Schematic of the simplified Cd_3As_2 structure derived from the antifluorite lattice. Indicated are empty sites on the cation sublattice (blue dashed lines) and the interstitial and vacancy defects. (b) DFT density of states for the V_{As}, V_{Cd}, and Cd_i defects, as a function of energy given relative to the Dirac point energy of the defect-free Cd_3As_2 host.

(distinct from empty sites) can form readily by either occupying these empty sites or removing existing Cd atoms, respectively. We additionally consider As vacancies (V_{As}), which have been tentatively implied as the source of electron doping in early investigations of Cd_3As_2 [35]. Figure 3(b) shows the calculated density of states (DOS) of these point defects. The DOS of V_{As} shows a localized defect state close to E_F, suggesting that V_{As} will cause electron scattering. This behavior is in agreement with scanning tunneling microscopy measurements, which showed that V_{As} caused fluctuations in conductance [32]. The V_{As} state is half filled, indicating that it has an amphoteric character and is not likely to be the source of free electrons. In contrast, V_{Cd} and Cd_i introduce hole and electron doping, respectively, without significantly changing the DOS profile of the defect-free crystal. Our calculations indicate (see SM [13] and Ref. [36]) that V_{As} has significantly higher formation energies than the Cd defects and thus will be several orders of magnitude lower in concentrations than those defects. Antisite defects and As interstitials have higher formation energies than V_{As} and have even lower concentrations. We expect that the V_{Cd} and Cd_i defects are the primary source of the disorder potential in Cd_3As_2. According to DFT for our growth conditions, the total concentration of V_{Cd} and Cd_i defects sum to $\sim10^{18}$ defects/cm^3, in agreement with Fig. 2(e). While we cannot directly probe the relative densities of V_{Cd} and Cd_i defects with the GCDM, the changes in n_{3D} as a function of As/Cd flux ratio are dependent on the relative concentrations of Cd_i and V_{Cd}. We are unlikely to see the effects of the changes in cadmium defect density on the mobility because our film mobilities are limited by extended defects. A more detailed DFT account of defects and doping in Cd_3As_2 is given in Ref. [36].

In summary, we find that the As/Cd flux ratio controls the concentration of point defects that contribute strongly to scattering. An order of magnitude reduction of the scattering center defect concentration as a function of As/Cd flux ratio paired with an increase in the disorder potential produces a substantial increase in the magnetoresistance from 450% to 900%. The onset of LMR, H_S, occurs at a lower field in the samples with fewer scattering centers. The As/Cd flux ratio controls the carrier concentration, which varies from 1

to 4×10^{17} cm^{-3}. By calculating defect concentrations with DFT, we link the scattering defects as well as variation of the carrier concentration to a combination V_{Cd} and Cd_i defects.

Our study reveals the connection between point defects and large LMR in Cd_3As_2. The importance of this work is summarized as follows. The tunable control of point defects made possible by MBE growth allows us to experimentally verify the ability of the GCDM to explain LMR behavior. Our findings represent widely applicable guidelines for engineering electronic properties within other topological semimetals. Since the mobility in our films is limited by extended defects, μ is decoupled from LMR, isolating the impact of point defects. We find that V_0 and E_{F} vary with the Cd defect concentrations, altering the LMR magnitude. This conclusion contradicts the previous assumption that V_{As} defects were responsible for LMR [10]. The verification of the GCDM as an experimental framework confirms the assertion that topological states are not responsible for LMR. Instead, LMR in Cd_3As_2 and similar systems is due to diffusive motion of charge carriers around potential barriers created by charged, screened point defects. Centrally, the GCDM connects a bulk magnetoelectric probe to details of microscopic disorder in TSMs. These results provide experimentally driven conclusions for the origin of LMR in TSMs and pave the way for the tunability and use of large LMR in device applications.

This research was performed in part under the project "Disorder in Topological Semimetals", funded by the U.S. Department of Energy (DOE), Office of Science (SC), Basic Energy Sciences, Physical Behavior of Materials program. The Alliance for Sustainable Energy, LLC, operates the National Renewable Energy Laboratory (NREL) for the DOE under contract No. DE-AC36-08GO28308. This research used High-Performance Computing (HPC) resources of the National Energy Research Scientific Computing Center (NERSC), a DOE-SC user facility located at Lawrence Berkeley National Laboratory, operated under Contract No. DE-AC02-05CH11231. This research also used HPC resources at NREL, sponsored by DOE, Office of Energy Efficiency and Renewable Energy. Guidance on the use of the GCDM (M.L.) was supported by an NSF Award No. DMR-2001376. The views expressed in the article do not necessarily represent the views of the DOE or the U.S. Government. The U.S. Government retains and the publisher, by accepting the article for publication, acknowledges that the U.S. Government retains a nonexclusive, paid-up, irrevocable, worldwide license to publish or reproduce the published form of this work, or allow others to do so, for U.S. Government purposes.

[1] L. M. Schoop, F. Pielnhofer, and B. V. Lotsch, Chemical principles of topological semimetals, Chem. Mater. **30**, 3155 (2018).

[2] T. Liang, Q. Gibson, M. N. Ali, M. Liu, R. J. Cava, and N. P. Ong, Ultrahigh mobility and giant magnetoresistance in the Dirac semimetal Cd_3As_2, Nat. Mater. **14**, 280 (2015).

[3] S. Singh, V. Süß, M. Schmidt, C. Felser, and C. Shekhar, Strong correlation between mobility and magnetoresistance in Weyl and Dirac semimetals, J. Phys. Mater. **3**, 024003 (2020).

[4] M. M. Parish and P. B. Littlewood, Classical magnetotransport of inhomogeneous conductors, Phys. Rev. B **72**, 094417 (2005).

[5] F. Kisslinger, C. Ott, and H. B. Weber, Origin of nonsaturating linear magnetoresistivity, Phys. Rev. B **95**, 024204 (2017).

[6] R. Nandkishore, D. A. Huse, and S. L. Sondhi, Rare region effects dominate weakly disordered three-dimensional Dirac points, Phys. Rev. B **89**, 245110 (2014).

[7] J. H. Pixley, D. A. Huse, and S. Das Sarma, Rare-Region-Induced Avoided Quantum Criticality in Disordered Three-Dimensional Dirac and Weyl Semimetals, Phys. Rev. X **6**, 021042 (2016).

[8] T. Holder, C.-W. Huang, and P. M. Ostrovsky, Electronic properties of disordered Weyl semimetals at charge neutrality, Phys. Rev. B **96**, 174205 (2017).

[9] B. Skinner, Coulomb disorder in three-dimensional Dirac systems, Phys. Rev. B **90**, 060202(R) (2014).

[10] A. Narayanan, M. D. Watson, S. F. Blake, N. Bruyant, L. Drigo, Y. L. Chen, D. Prabhakaran, B. Yan, C. Felser, T. Kong, P. C. Canfield, and A. I. Coldea, Linear Magnetoresistance Caused by Mobility Fluctuations in *n*-Doped Cd_3As_2, Phys. Rev. Lett. **114**, 117201 (2015).

[11] J. C. W. Song, G. Refael, and P. A. Lee, Linear magnetoresistance in metals: Guiding center diffusion in a smooth random potential, Phys. Rev. B **92**, 180204(R) (2015).

[12] A. A. Abrikosov, Quantum magnetoresistance, Phys. Rev. B **58**, 2788 (1998).

[13] See Supplemental Material at http://link.aps.org/supplemental/10.1103/PhysRevB.107.L220206 for additional details on thin-film synthesis, x-ray photoemission spectroscopy, temperature-dependent resistivity and mobility, Fourier transforms of the quantum oscillations, additional information on quasiparticle self-consistent *GW* (QS*GW*) and DFT calculations, and an expanded discussion of the guiding center diffusion model.

[14] G. Kresse and D. Joubert, From ultrasoft pseudopotentials to the projector augmented-wave method, Phys. Rev. B **59**, 1758 (1999).

[15] J. Sun, A. Ruzsinszky, and J. P. Perdew, Strongly Constrained and Appropriately Normed Semilocal Density Functional, Phys. Rev. Lett. **115**, 036402 (2015).

[16] J. Sun, M. Marsman, G. I. Csonka, A. Ruzsinszky, P. Hao, Y.-S. Kim, G. Kresse, and J. P. Perdew, Self-consistent meta-generalized gradient approximation within the projector-augmented-wave method, Phys. Rev. B **84**, 035117 (2011).

[17] A. Chakraborty, M. Dixit, D. Aurbach, and D. T. Major, Predicting accurate cathode properties of layered oxide materials using the scan meta-GGA density functional, npj Comput. Mater. **4**, 60 (2018).

[18] L. Galletti, T. Schumann, T. E. Mates, and S. Stemmer, Nitrogen surface passivation of the Dirac semimetal Cd_3As_2, Phys. Rev. Mater. **2**, 124202 (2018).

[19] M. van Schilfgaarde, T. Kotani, and S. Faleev, Quasiparticle Self-Consistent *GW* Theory, Phys. Rev. Lett. **96**, 226402 (2006).

[20] T. Kotani, M. van Schilfgaarde, and S. V. Faleev, Quasiparticle self-consistent *GW* theory, Phys. Rev. B **76**, 165106 (2007).

[21] M. van Schilfgaarde and M. I. Katsnelson, First-principles theory of nonlocal screening in graphene, Phys. Rev. B **83**, 081409(R) (2011).

[22] B. Cunningham, M. Gruening, D. Pashov, and M. van Schilfgaarde, QSGW: Quasiparticle Self consistent *GW* with ladder diagrams in *W*, arXiv:2106.05759.

[23] A. N. Chantis, M. van Schilfgaarde, and T. Kotani, *Ab initio* Prediction of Conduction Band Spin Splitting in Zinc Blende Semiconductors, Phys. Rev. Lett. **96**, 086405 (2006).

[24] D. Deguchi, K. Sato, H. Kino and T. Kotani, Accurate energy bands calculated by the hybrid quasiparticle self-consistent *GW* method implemented in the ecalj package, Jpn. J. Appl. Phys. **55**, 051201 (2016).

[25] M. M. Fogler, A. Yu. Dobin, V. I. Perel and B. I. Shklovskii, Suppression of chaotic dynamics and localization of two-dimensional electrons by a weak magnetic field, Phys. Rev. B **56**, 6823 (1997).

[26] D. G. Polyakov, Change, due to scattering-act correlation, of electron diffusion in a classically strong magnetic field, Zh. Eksp. Teor. Fiz. **90**, 546 (1986) [Sov. Phys. JETP **63**, 317 (1986)].

[27] A. D. Rice, K. Park, E. T. Hughes, K. Mukherjee, and K. Alberi, Defects in Cd_3As_2 epilayers via molecular beam epitaxy and strategies for reducing them, Phys. Rev. Mater. **3**, 121201(R) (2019).

[28] O. F. Shoron, D. A. Kealhofer, M. Goyal, T. Schumann, A. A. Burkov, and S. Stemmer, Detecting topological phase transitions in cadmium arsenide films via the transverse magnetoresistance, Appl. Phys. Lett. **119**, 171907 (2021).

[29] Y. Nakazawa, M. Uchida, S. Nishihaya, S. Sato, A. Nakao, J. Matsuno, and M. Kawasaki, Molecular beam epitaxy of three-dimensionally thick Dirac semimetal Cd_3As_2 films, APL Mater. **7**, 071109 (2019).

[30] L. P. He, X. C. Hong, J. K. Dong, J. Pan, Z. Zhang, J. Zhang, and S. Y. Li, Quantum Transport Evidence for the Three-Dimensional Dirac Semimetal Phase in Cd_3As_2, Phys. Rev. Lett. **113**, 246402 (2014).

[31] I. A. Leahy, Y.-P. Lin, P. E. Siegfried, A. C. Treglia, J. C. W. Song, R. M. Nandkishore, and M. Lee, Nonsaturating large magnetoresistance in semimetals, Proc. Natl. Acad. Sci. USA **115**, 10570 (2018).

[32] S. Jeon, B. B. Zhou, A. Gyenis, B. E. Feldman, I. Kimchi, A. C. Potter, Q. D. Gibson, R. J. Cava, A. Vishwanath, and A. Yazdani, Landau quantization and quasiparticle interference in the three-dimensional Dirac semimetal Cd_3As_2, Nat. Mater. **13**, 851 (2014).

[33] M. T. Edmonds, J. L. Collins, J. Hellerstedt, I. Yudhistira, L. C. Gomes,J. N. B. Rodrigues,S. Shaffique, and M. S. Fuhrer, Spatial charge inhomogeneity and defect states in topological Dirac semimetal thin films of Na_3Bi, Sci. Adv. **3**, eaao6661 (2017).

[34] M. N. Ali, Q. Gibson, S. Jeon, B. B. Zhou, A. Yazdani, and R. J. Cava, The Crystal and Electronic Structures of Cd_3As_2, the Three-Dimensional Electronic Analogue of Graphene, Inorg. Chem. **53**, 4062 (2014).

[35] D. P. Spitzer, G. A. Castellion, and G. Haacke, Anomalous Thermal Conductivity of Cd_3As_2 and the Cd_3As_2-Zn_3As_2 Alloys, J. Appl. Phys. **37**, 3795 (1966).

[36] C. Brooks, M. van Schilfgaarde, D. Pashov, J. N. Nelson, K. Alberi, D. S. Dessau, and S. Lany, Band energy dependence of defect formation in the topological semimetal Cd_3As_2, Phys. Rev. B **107**, 224110 (2023).